The contribution of propagons and diffusons in heat transport through calcium-silicate-hydrates

Yun Zhou, Ali Morshedifard, Jaeho Lee, and Mohammad Javad Abdolhosseini Qomi

Citation: Appl. Phys. Lett. **110**, 043104 (2017); doi: 10.1063/1.4975159
View online: http://dx.doi.org/10.1063/1.4975159
View Table of Contents: http://aip.scitation.org/toc/apl/110/4
Published by the American Institute of Physics

The contribution of propagons and diffusons in heat transport through calcium-silicate-hydrates

Yun Zhou,[1] Ali Morshedifard,[1] Jaeho Lee,[2] and Mohammad Javad Abdolhosseini Qomi[1,a)]
[1]*Department of Civil and Environmental Engineering, Henry Samuelli School of Engineering, University of California, Irvine, California 92617, USA*
[2]*Department of Mechanical and Aerospace Engineering, Henry Samuelli School of Engineering, University of California, Irvine, California 92617, USA*

(Received 6 October 2016; accepted 18 January 2017; published online 26 January 2017)

Whether it is glass, ceramics, cement, or concrete, minimizing thermal conduction through disordered materials is a determining factor when it comes to reducing the energy consumption of cities. In this work, we explore underlying physical processes involved in thermal conduction through the disordered glue of cement, calcium-silicate-hydrates (CSH). We find that at 300 K, phonon-like propagating modes in accordance with the Boltzmann transport theory, propagons, account for more than 30% of the total thermal conductivity, while diffusons, described via the Allen-Feldman theory, contribute to the remainder. The cumulative thermal conductivity proves to be close to both equilibrium molecular dynamics calculations and experimental values. These findings help us establish different strategies, such as localization schemes (to weaken diffusons) and scattering mechanisms (to constrain propagons), for reduction of thermal conductivity of CSH without sacrificing its mechanical properties. *Published by AIP Publishing.*
[http://dx.doi.org/10.1063/1.4975159]

Minimizing thermal conduction in buildings proves to be indispensable when it comes to reducing the energy consumption and carbon footprint of cities.[1] The thermal conduction through disordered materials, e.g., glass, ceramics, cement, and concrete, dominates this massive energy loss, yet we have not found effective ways to reduce their thermal conductivity. For instance, increasing cement's porosity lowers its thermal conductivity, while this significantly decreases its mechanical properties. In a community driven by interest in superior strength and stiffness,[2–5] it is imperative to seek solutions that reduce the thermal conductivity of the construction material without decreasing its mechanical properties. In the glass community, researchers[6–13] have shown that both phonon-like propagating modes (propagons) and diffusive modes (diffusons) contribute significantly to the thermal conductivity. This motivates us to obtain an in depth understanding of cement's heat transport, in terms of propagon and diffuson contributions. In this letter, we employ computational physics tools such as molecular dynamics, lattice dynamics, Boltzmann transport equation (BTE), and Allen-Feldman (AF) theory,[8] to probe the fundamental mechanisms of heat transport in calcium-silicate-hydrates (CSH), the binding phase of cement, at the atomic level. This helps us propose different strategies to effectively reduce the thermal conductivity of this class of disordered materials.

The molecular structure of CSH has been the subject of extensive research in the past decade.[2,14–16] The proposed structures are produced by introducing vacancy defects in drierketten silicate chains of Tobermorite minerals.[17] Here, we use the molecular structure containing 501 atoms proposed by Qomi *et al.*,[2] which is in agreement with a variety of analytical experiments. As depicted in Fig. 1(a), CSH's structure is composed of intra-layer calcium oxide layers tethered by broken tetrahedral silicate chains. These defective calcium-silicate layers are negatively charged and are neutralized by inter-layer calcium ions. The inter-laminar spacing is also filled with nano-confined water that screens ionic correlation forces and exhibits composition-dependent anomalous glassy behavior.[3,18] Here, the inter- and intra-molecular interactions are described using core-only CSH-force filed potential.[19] We use large-scale atomic/molecular massively parallel simulator package in all MD simulations[20] and adopt the Velocity Verlet finite difference algorithm with 0.1 fs time step to fully resolve dynamics of O-H bonds. Initially, we perform a single MD simulation in canonical ensemble (NVT) using a Nosè-Hoover thermostat at $T = 300$ K for 1 ns. Subsequently, we sample at 5 statistically independent points along the NVT trajectory and run 5 ns-long simulations in micro-canonical ensemble (NVE) to record coordinates, velocities, and kinetic and potential energies as well as heat fluxes in adequate intervals.

To calculate the thermal conductivity of CSH, κ_{GK}, we use the Green-Kubo method within the equilibrium MD (EMD) approach,

$$\kappa_{GK} = \frac{V}{3k_B T^2}\int_0^\infty \langle \vec{J}_0 \cdot \vec{J}_\tau \rangle d\tau, \tag{1}$$

where $\vec{J}_\tau$ is the volumetric heat flux vector at time τ, k_B is the Boltzmann constant, V is the simulation cell volume, and $\langle . \rangle$ denotes an average over time.[21] Fig. 1(b) provides the heat flux autocorrelation function (HFACF) and Green-Kubo thermal conductivity for CSH. We find the average thermal conductivity of CSH to be roughly 1.0 W/mK. Convergence studies on $2 \times 1 \times 1$, $2 \times 2 \times 1$, and $2 \times 2 \times 2$ supercells indicate that Green-Kubo results are not size dependent as the medium-range order in our amorphous system is considerably

a)Electronic mail: mjaq@uci.edu

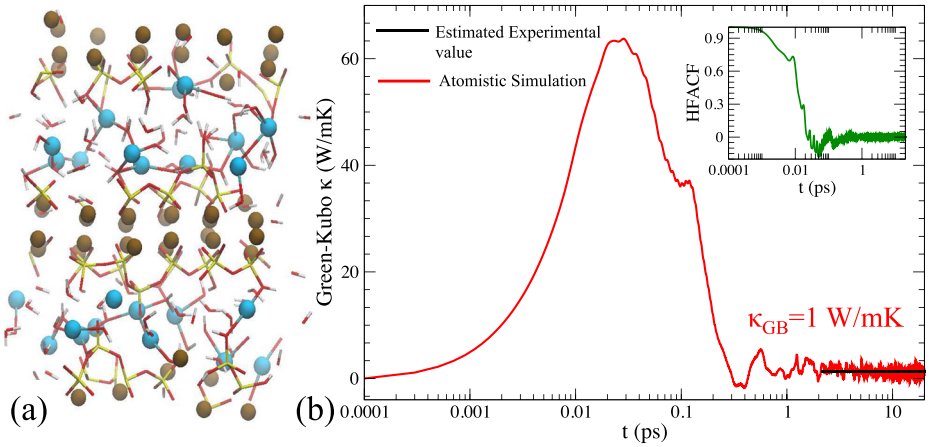

FIG. 1. The molecular structure and thermal conductivity of CSH at 300 K. (a) The atomic structure of glassy CSH at Ca/Si = 1.7. Silicon, oxygen, hydrogen, intra- and inter-layer calcium atoms are, respectively, shown in yellow, red, white, brown and cyan. (b) CSH thermal conductivity predicted by equilibrium molecular dynamics' Green-Kubo approach. The value is in agreement with the homogenization-based inverse estimates, which is also shown in the plot. The inset shows that the normalized heat flux autocorrelation function (HFACF) goes to zero after 2 ps, indicating that MD simulation reaches equilibrium.

smaller than the smallest side of the unit cell, see supplementary material. These results are in agreement with homogenization-based inverse estimates calculated from macroscopic thermal conduction measurements.[22] However, our EMD analysis does not provide the necessary description of underlying physics of heat carriers in CSH and hence fails to provide effective approaches to reduce its thermal conductivity.

To this end, we resort to mode-dependent thermal conductivity approaches to measure the contribution of each phonon in overall thermal conductivity. Based on the single mode relaxation time approximation (SMRT),[23] we can describe the thermal conductivity of a system via the Boltzmann transport equation (BTE),

$$\kappa_{\mathrm{BTE}} = \frac{1}{V}\sum_i C_i v_i^2 \tau_i, \tag{2}$$

where C_i, v_i, and τ_i are, respectively, the specific heat, group velocity, and relaxation time of the ith vibrational mode. Here, we use the classic harmonic limit of specific heat, $C_i = k_{\mathrm{B}}$. To calculate the vibrational density of states (VDOS), VDOS(ν), we use both Fourier transformation of the velocity autocorrelation function (VACF) over EMD trajectories and the eigenvalue decomposition of the dynamical matrix (EDDM).[22] The eigenvalues and eigenvectors are calculated using general utility lattice program (GULP) lattice dynamics software.[24,25] Fig. 2(a) presents almost identical result of VDOS for CSH from VACF and EDDM approaches. We note that at low frequencies, VDOS scales with ν^2, $\mathrm{VDOS}(\nu) = \frac{6V\nu^2}{v_a^3}$, in agreement with the Debye model, where V is the volume of the system and v_a is the acoustic velocity.

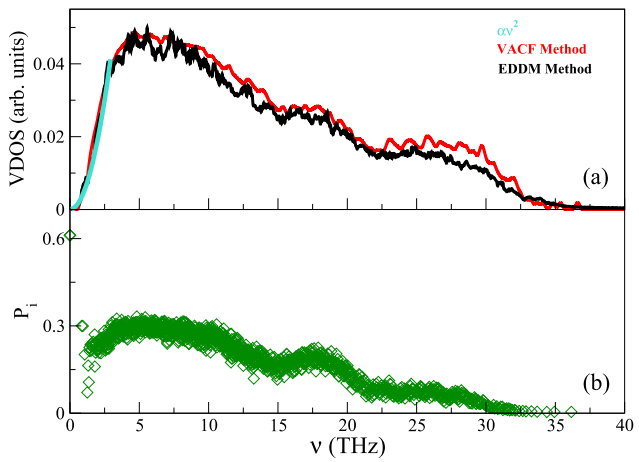

FIG. 2. Analysis of phonons in CSH. (a) Vibrational Density of States (VDOS) of CSH calculated via the eigenvalue decomposition of the dynamical matrix (EDDM), and Fourier transformation of the velocity autocorrelation function (VACF). The blue line indicates a ν^2 scaling at low frequency. (b) Participation ratio P_i of the vibrational modes, which indicates the fraction of atoms vibrating in a given vibrational frequency. Modes associated with O-H bonds are not included in the figure.

For a disordered system, even at low frequencies, most of the vibrational modes cannot be properly assigned a unique wave vector, making it hard to predict the group velocity for each individual mode. Except for acoustic modes, there is no widely accepted way to predict the group velocity for a disordered system. The longitudinal and transverse acoustic velocities from the slope of the dispersion curves at the gamma point are reported in Table I. These results are in complete agreement with the acoustic velocities calculated from the bulk and shear moduli,[25,26] see Table I for comparison. The transverse and longitudinal acoustic velocities yield the average acoustic velocity,[27] $v_a = \left[\frac{1}{3}\left(\frac{1}{v_l^3} + \frac{2}{v_t^3}\right)\right]^{-\frac{1}{3}}$. To obtain a qualitative understanding of group velocities at high frequencies, we calculate the conventional "*dispersion group velocity*," via the forward finite difference technique at the gamma point, see supplementary material for details. To investigate the thermal activation degree of phonons, we compute the participation ratio of each vibrational mode.[28] This ratio characterizes the fraction of atoms that vibrate at a given vibrational mode. It can be expressed as $\frac{1}{\mathrm{P}_i} = N\sum_n\left[\sum_\alpha\left(e^*_{\alpha,n}(i)\, e_{\alpha,n}(i)\right)\right]^2$, where N is the total number of atoms and $e_{\alpha,n}(i)$ is the αth coordinate component of the normalized eigenvector corresponding to the ith eigenmode of atom n. Fig. 2(b) shows that for acoustic modes where frequency equals zero, over 60% of atoms participate in the vibration, which is nearly the entire structure minus nano-confined water

TABLE I. Longitudinal and transverse acoustic velocities for CSH obtained from the dispersion relation and the elastic moduli.

Method	v_l	v_t
Dispersion relation	6286	3167
Elastic moduli	6012	3224

molecules and hydroxyl groups. However, as the frequency increases, P_i decreases gradually to zero. Similar behavior is also reported for other disordered systems.[7,11] Such an observation already signals that phonon propagation might not be sufficient to describe thermal conduction in CSH.

Following Larkin and McGaughey[11] we calculate the phonon relaxation time, τ_i, using Lorentzian fit of phonon spectral energy density function (SEDF).[11] Fig. 3(a) shows computed phonon relaxation time of each vibrational mode in CSH. The low frequency τ scales with ν^{-2}, while higher frequencies roughly follow a ν^{-1} trend. The ν^{-2} scaling of the relaxation time has also been observed in experiments and other theoretical studies for crystals, as a result of anharmonic scattering.[26,29] If we compute the thermal conductivity of CSH by substituting the dispersion group velocity and the relaxation time of each vibrational mode into Eq. (2), we get a thermal conductivity value that is an order of magnitude less than EMD, $\kappa_{BTE} \ll \kappa_{GB}$. This is not only because the dispersion group velocities we get from the dispersion relation cannot be treated as the actual group velocity for our disordered system but also because there exist nonpropagating vibrations that do not propagate but carry heat diffusively.[6,7] This already suggests that the thermal conduction can be decomposed into propagating, κ_{pr}, and diffusive, κ_{dif}, contributions,

$$\kappa_{vib} = \kappa_{pr} + \kappa_{dif}. \tag{3}$$

The contribution to thermal conductivity from diffusons can be computed using the Allen-Feldman (AF) theory,[7,9]

$$\kappa_{dif} = \frac{1}{V}\sum_i C(\nu_i) D_{dif}(\nu_i), \tag{4}$$

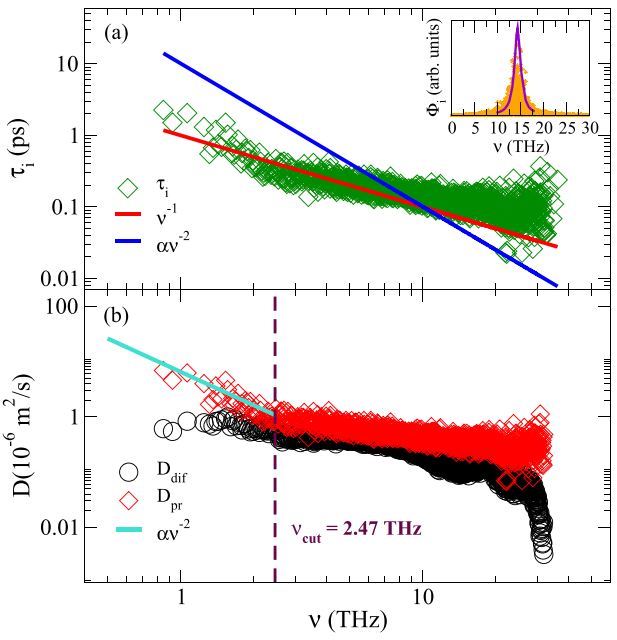

FIG. 3. Phonon relaxation time and mode diffusivity in CSH. (a) Relaxation time of each vibrational mode τ_i calculated from fitting phonon spectral energy density function (SEDF). τ_i scales with ν^{-2} at low frequencies and shows a scaling that is closer to ν^{-1} at higher frequencies. The inset shows the Lorentzian fit of the SEDF at a certain vibrational mode. (b) Propagating mode diffusivity D_{pr} and nonpropagating mode diffusivity D_{dif} for each vibrational mode. D_{pr} also shows a ν^{-2} scaling for the low-frequency region. We present results for three cut-off frequencies of 2.2, 2.47, and 2.8 THz that separate propagons and diffusons.

where $D_{dif}(\nu_i)$ is the nonpropagating mode diffusivity. It is given by[6] $D_{dif}(\nu_i) = \frac{\pi V^2}{h^2 \nu_i^2}\sum_{j\neq i}|S_{ij}|^2 \delta(\nu_i - \nu_j)$, where h is the Planck constant, S_{ij} is the heat current operator, and δ is the Dirac delta function. In our calculation, $D_{dif}(\nu_i)$ is obtained by GULP and a Lorentzian broadening of $2\delta\omega_{avg}$, where $\delta\omega_{avg}$ is the average mode frequency spacing of CSH. To compensate for the simulation box size effect, we use the integral expression of solution to the BTE equation to describe propagons,[7,12,30]

$$\kappa_{pr} = \frac{2\pi}{V}\int_0^{\nu_{cut}} \mathrm{VDOS}(\nu) C(\nu) D_{pr}(\nu) d\nu. \tag{5}$$

Here, ν_{cut} is the highest frequency at which modes propagate. D_{pr} is the propagating mode diffusivity, $D_{pr}(\nu) = \frac{1}{3} v_a^2 \tau(\nu)$. This expression is obtained by the phonon-gas model within the SMRT approximation, and it allows us to model modes that fall in the low-frequency region through an extrapolation scheme. This eliminates the need to measure properties of vibrational modes near the gamma point.[7,11]

The propagating mode diffusivity, D_{pr}, and nonpropagating mode diffusivity, D_{dif}, of CSH are calculated for all vibrational frequencies, Fig. 3(b). D_{pr} is equal or greater than D_{dif} for all modes, and it follows the same scaling relation as the relaxation time τ_i in Fig. 3(a). Here, we consider modes whose relaxation times scale with ν^{-2} as propagons, and model τ as

$$\tau(\nu) = \beta \nu^{-2}, \tag{6}$$

where β is a temperature-dependent constant. Here, for CSH at 300 K, $\beta = 3.81 \times 10^{14}\ \mathrm{s}^{-1}$. We set the cut-off frequency ν_{cut} to be 2.47 THz, where the average values of D_{pr} and D_{dif} start to become very close to each other. Furthermore, the cut-off frequency lies in the range (2.2–2.8 THz) in which we observe the slope change in mean relaxation time, Fig. 3(a). This frequency also falls at the far right side of Debye frequency range. There is an uncertainty associated with the determination of cut-off frequency as it is not a clear cut value. Nevertheless, we find that the value of the total thermal conductivity is hardly affected when we move the cut-off point within a reasonable range (2.5 ± 0.3 THz). We treat modes with $\nu \leqslant 2.47$ THz as propagons and compute their contribution to the thermal conductivity using Eq. (5). For $\nu > 2.47$ THz, modes are considered as diffusons, and we employ Eq. (4) to predict their thermal conductivity contribution. The cumulative thermal conductivity of CSH in the frequency domain is presented in Fig. 4(a). κ_{vib} is slightly smaller than κ_{GK}, but the difference is within uncertainties caused by the choice of ν_{cut}, the AF broadening factor, and neglecting the contribution of the nano-confined water in the inter-laminar spacing. From our calculations, it turns out that more than 30% of the thermal conductivity of CSH comes from propagons, while 70% is attributed to the contribution from diffusons. Our convergence study shows that κ_{vib} is not affected by the size of the simulation box, see supplementary material.

Incorporating macroscale porosity in the CSH matrix is the traditional approach to decrease its thermal conductivity. According to the mean field homogenization theory,[22,32,33] also known as the effective medium theory, both bulk

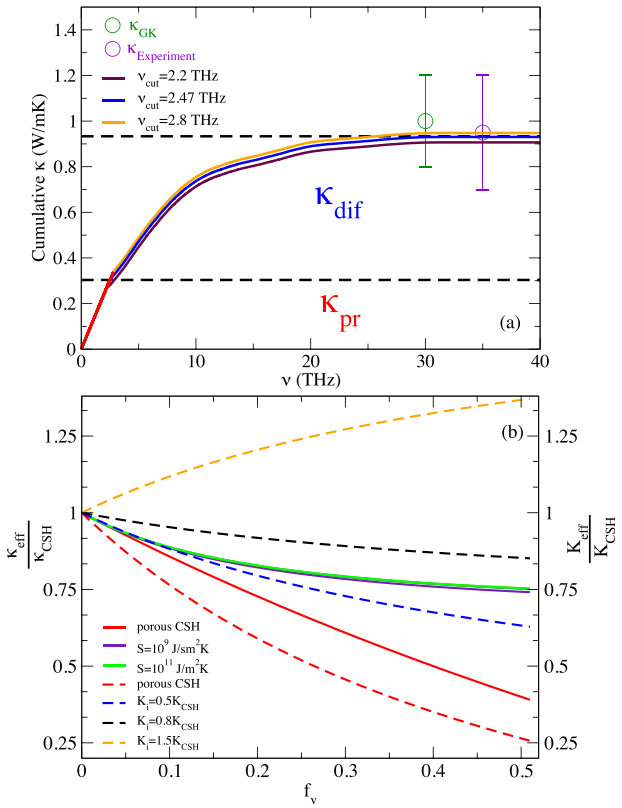

FIG. 4. (a) Cumulative thermal conductivity of CSH computed combining the contribution from Boltzmann transport equation for the modes with frequency lower than 2.47 THz, propagons, and the Allen and Feldman model for modes with frequency higher than 2.47 THz, diffusons. Also shown in the figure are the thermal conductivity values from the MD Green-Kubo approach and experiment with error bars. The experimental result is derived from inverse homogenization of macroscopic thermal conduction measurements.[22,31] (b) The comparison of effects of macro void inclusion and nanoparticle inclusion on the thermal conductivity and elastic bulk modulus of CSH. Thermal conductivity and bulk modulus are shown in solid and dashed lines, respectively.

modulus and thermal conductivity of CSH decrease with increasing pore volume fraction, see Fig. 4(b) and supplementary material for details. Here, we propose an alternative approach to tune the thermal conductivity of CSH without losing its stiffness properties. We can diminish the contribution of propagons by exploiting the notion of the size effect. Such solutions effectively reduce the mean free path of propagons, $\Lambda^i_{\text{pr–pr}}$, by scattering the low-frequency acoustic waves. In practice, we can achieve this by mixing CSH with mismatch nanoparticles with the condition that their mean separation distance, $\bar{\Lambda}_{\text{sep}}$, is comparable to the propagon mean free path, $\bar{\Lambda}_{\text{sep}} < \Lambda_{\text{pr–pr}}$. Assuming that propagon-propagon scattering and propagon-nanoparticle scattering are statistically independent processes, the Matthiessen rule[34] provides their combined action as follows:

$$\frac{1}{\Lambda^i_{\text{eff}}} = \frac{1}{\bar{\Lambda}_{\text{sep}}} + \frac{1}{\Lambda^i_{\text{pr–pr}}}, \tag{7}$$

where Λ^i_{eff} is the effective mean free path of the ith propagating mode located in the low-frequency acoustic region. Assuming spherical nanoparticles with diameter of a few nanometers and bulk mean free path of phonons much greater than their diameters, then according to the modified effective medium theory,[35] the effective thermal conductivity becomes a function of the inclusion S parameter, $S = C_{\text{np}} v_{\text{np}}$, where C_{np} and v_{np} are, respectively, the volumetric specific heat and phonon group velocity of the nanoparticle. Fig. 4(b) shows the effect of nanoparticle inclusions of 2 nm diameter with $S = 10^9$ and $10^{11}\text{J/sm}^2\text{K}$. The increase in volume fraction of nanoparticles, f_v, decreases the contribution of the propagons and the thermal conductivity as a result, while nanoparticles' S parameter does not alter thermal conductivity significantly. If we choose nanoparticles that render higher bulk modulus K_{i} than CSH, the effective bulk modulus can be increased by nanoparticle inclusions. Therefore, by adding appropriate nanoparticles into the CSH system, both thermal and mechanical properties can be improved. Based on the effective medium theory, if we fabricate such a nanocomposite, the aforementioned scattering mechanism would only reduce $\kappa_{\text{pr}} \approx 0.3\kappa_{\text{vib}}$. However, the presence of nanoparticles might further alter propagon-diffuson population and subsequently affect the mode-nanoparticle interaction. This would potentially decrease the thermal conductivity below the amorphous limit and requires full atomistic simulation for further verification. Furthermore exploiting the ideas in topological constraints theory[36] and dopant-induced phonon localization[37] might prove to be worthwhile venues to reduce κ_{dif}.

See supplementary material for more details on simulation convergence, dispersion curves, and effective medium theory.

[1]M. J. A. Qomi, A. Noshadravan, J. M. Sobstyl, J. Toole, J. Ferreira, R. J.-M. Pellenq, F.-J. Ulm, and M. C. Gonzalez, J. R. Soc. Interface **13**, 20150971 (2016).
[2]M. J. Abdolhosseini Qomi, K. J. Krakowiak, M. Bauchy, K. L. Stewart, R. Shahsavari, D. Jagannathan, D. B. Brommer, A. Baronnet, M. J. Buehler, S. Yip, F.-J. Ulm, K. J. Van Vliet, and R. J.-M. Pellenq, Nat. Commun. **5**, 4960 (2014).
[3]M. J. A. Qomi, M. Bauchy, F.-J. Ulm, and R. J.-M. Pellenq, J. Chem. Phys. **140**, 054515 (2014).
[4]M. Bauchy, M. J. A. Qomi, F.-J. Ulm, and R. J.-M. Pellenq, J. Chem. Phys. **140**, 214503 (2014).
[5]M. Bauchy, H. Laubie, M. J. Abdolhosseini Qomi, C. G. Hoover, F. J. Ulm, and R. J. M. Pellenq, J. Non-Cryst. Solids **419**, 58 (2015).
[6]P. B. Allen and J. L. Feldman, Phys. Rev. B **48**, 12581 (1993).
[7]J. L. Feldman, M. D. Kluge, P. B. Allen, and F. Wooten, Phys. Rev. B **48**, 12589 (1993).
[8]P. B. Allen, J. L. Feldman, J. Fabian, and F. Wooten, Philos. Mag. Part B **79**, 1715 (1999).
[9]J. L. Feldman, P. B. Allen, and S. R. Bickham, Phys. Rev. B **59**, 3551 (1999).
[10]D. Donadio and G. Galli, Phys. Rev. Lett. **102**, 195901 (2009).
[11]J. M. Larkin and A. J. H. McGaughey, Phys. Rev. B **89**, 144303 (2014).
[12]T. Zhu and E. Ertekin, Phys. Rev. B **93**, 155414 (2016).
[13]M. C. Wingert, J. Zheng, S. Kwon, and R. Chen, Semicond. Sci. Technol. **31**, 113003 (2016).
[14]R. J.-M. Pellenq, A. Kushima, R. Shahsavari, K. J. V. Vliet, M. J. Buehler, S. Yip, and F.-J. Ulm, Proc. Natl. Acad. Sci. **106**, 16102 (2009).
[15]L. B. Skinner, S. R. Chae, C. J. Benmore, H. R. Wenk, and P. J. M. Monteiro, Phys. Rev. Lett. **104**, 195502 (2010).
[16]H. Manzano, S. Moeini, F. Marinelli, A. C. T. van Duin, F.-J. Ulm, and R. J.-M. Pellenq, J. Am. Chem. Soc. **134**, 2208 (2012).
[17]I. G. Richardson, Cem. Concr. Compos. **22**, 97 (2000).
[18]M. Youssef, R. J.-M. Pellenq, and B. Yildiz, J. Am. Chem. Soc. **133**, 2499 (2011).
[19]R. Shahsavari, R. J.-M. Pellenq, and F.-J. Ulm, Phys. Chem. Chem. Phys.: PCCP **13**, 1002 (2011).
[20]S. Plimpton, J. Comput. Phys. **117**, 1 (1995).

[21]P. K. Schelling, S. R. Phillpot, and P. Keblinski, Phys. Rev. B **65**, 144306 (2002).
[22]M. J. Abdolhosseini Qomi, F.-J. Ulm, and R. J.-M. Pellenq, Phys. Rev. Appl. **3**, 064010 (2015).
[23]A. J. H. McGaughey and M. Kaviany, Phys. Rev. B **69**, 094303 (2004).
[24]J. D. Gale, J. Chem. Soc.-Faraday Trans. **93**, 629 (1997), wOS:A1997WK27100016.
[25]J. D. Gale and A. L. Rohl, Mol. Simul. **29**, 291 (2003).
[26]T. M. Tritt, *Thermal Conductivity: Theory, Properties, and Applications* (Springer Science & Business Media, 2005).
[27]S. Bhowmick and V. B. Shenoy, J. Chem. Phys. **125**, 164513 (2006).
[28]T. Zhu and E. Ertekin, Nano Lett. **16**, 4763 (2016).
[29]J. Callaway, Phys. Rev. **113**, 1046 (1959).
[30]A. S. Henry and G. Chen, J. Comput. Theor. Nanosci. **5**, 141 (2008).
[31]D. P. Bentz, Mater. Struct. **40**, 1073 (2007).
[32]T. Mori and K. Tanaka, Acta Metal. **21**, 571 (1973).
[33]H. Hatta and M. Taya, J. Appl. Phys. **58**, 2478 (1985).
[34]J. M. Ziman, *Electrons and Phonons: The Theory of Transport Phenomena in Solids*, 1st ed. (Oxford University Press, New York, NY, 2001).
[35]A. Minnich and G. Chen, Appl. Phys. Lett. **91**, 073105 (2007).
[36]M. Bauchy, M. J. A. Qomi, C. Bichara, F.-J. Ulm, and R. J.-M. Pellenq, Phys. Rev. Lett. **114**, 125502 (2015).
[37]S. Pailhs, H. Euchner, V. Giordano, R. Debord, A. Assy, S. Goms, A. Bosak, D. Machon, S. Paschen, and M. de Boissieu, Phys. Rev. Lett. **113**, 025506 (2014).